Charged-particle emission in reactions of 15-MeV neutrons with isotopes of chromium, iron, nickel, and copper

S. M. Grimes* and R. C. Haight

Lawrence Livermore Laboratory, Livermore, California 94550

K. R. Alvar,[†] H. H. Barschall, and R. R. Borchers[‡]

University of Wisconsin, Madison, Wisconsin 53706

(Received 31 October 1978)

Cross sections have been measured for the emission of protons, deuterons, and alpha particles for 15-MeV neutrons on ^{54,56}Fe, ^{58,60}Ni, ^{50,52}Cr, and ^{63,65}Cu, as well as on natural iron, nickel, and chromium. A quadrupole spectrometer served to detect particles with energies as low as 1 MeV. For some of the targets, a substantial fraction of the charged-particle spectrum is at energies below the Coulomb barrier. Cross sections and spectra are compared with statistical and pre-equilibrium model predictions.

NUCLEAR REACTIONS ^{50,52}Cr, Cr, ^{54,56}Fe, Fe, ^{58,60}Ni, Ni, ^{63,65}Cu, (n,p), (n,d), (n,α), $E = 14.8$ MeV; measured $\sigma(E_p, \theta)$, (E_d, θ), (E_α, θ), enriched and natural targets. Hauser-Feshbach analysis, deduced reaction mechanism.

I. INTRODUCTION

Cross sections for the emission of protons, deuterons, and alpha particles in reactions of neutrons near 14 MeV are of interest for both basic and applied nuclear physics. Recent measurements[1,2] of these cross sections for ^{27}Al, ^{46}Ti, and ^{48}Ti and for ^{51}V and ^{93}Nb have illuminated aspects of the reaction mechanism. In particular, these data indicated that charged particles with energies below the Coulomb barrier can be emitted with high probability in the decay of an excited nucleus if other modes of decay are inhibited. In previous studies, especially large effects were found in the proton spectra if the target nucleus has a neutron binding energy that is larger than the proton binding energy. In this case there are excited states of the target that cannot decay by neutron emission but that can emit a low-energy proton. Since γ-ray emission is the only alternative decay channel, proton decay is usually the preferred mode even if the available energy is less than the Coulomb barrier. For example, in ^{46}Ti, where the last neutron is bound more tightly than the last proton by nearly 3 MeV, the cross section for the emission of sub-Coulomb-barrier protons is more than a third of the total proton-emission cross section. For ^{48}Ti, on the other hand, where the binding energies are nearly equal, the number of protons with energies below the Coulomb barrier is smaller by more than an order of magnitude.

For applied purposes, the measurement of hydrogen and helium production is important in assessing radiation damage of materials for fusion reactors. Hydrogen and helium produced in reactions

of 14-MeV neutrons alter the mechanical properties of materials. This source of radiation damage occurs in addition to the radiation damage caused by displacements of atoms by neutrons and the secondary charged particles.

A better understanding of the reaction mechanism will help in predicting the reaction cross sections for nuclides for which no direct measurements are available. In particular a knowledge of the charged-particle spectra and angular distributions can serve to check the validity of the calculations, although the total cross sections for hydrogen and helium production are most important for estimating radiation damage effects.

The measurements of charged-particle emission are related to radiochemical studies in that complementary reaction products are investigated. A complicating feature, however, is that, for all of the targets studied here, several channels are open for reactions induced by neutrons near 14 MeV. The proton-emission cross section is the sum of (n,p), (n,np), and possibly other channels, depending on the reaction Q value. For alpha-particle emission, the emission cross section again is a sum, usually of the (n,α) and $(n,n\alpha)$ cross sections. Deuteron emission is simpler, however, since the large negative Q values effectively limit it to (n,d) only. Radiochemical data can be used to identify some of these competing channels, although certain channels such as (n,np) and (n,d) lead to the same residual nucleus and therefore cannot be separated radiochemically.

There are several advantages of the present method over radiochemical measurements: For most target nuclides some of the charged-particle-
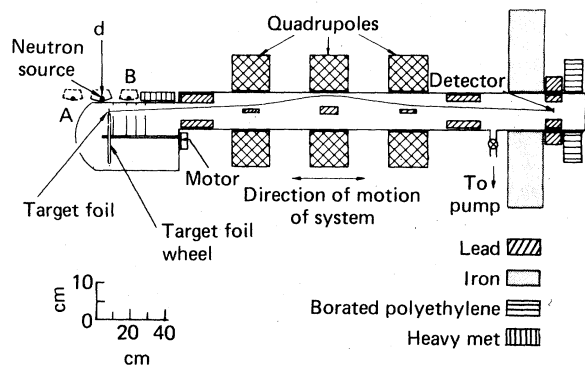
FIG. 1. Detection system for charged particles produced by neutrons. A typical trajectory of a charged particle from a neutron-induced reaction is shown. The entire system can be moved parallel to its axis so that charged particles emitted at different angles with respect to the incident neutron direction can be observed. Position A of the neutron source relative to the target foil corresponds to a reaction angle less than 90° and position B to an angle greater than 90°.

emission channels lead to nuclides that are stable and hence are not accessible to radiochemical measurements. In addition, the radiochemical measurements do not yield cross sections as a function of outgoing energy or angle, information that, in addition to its usefulness in estimating nuclear recoil energies in the lattice, is valuable in testing nuclear models. Furthermore, some reaction channels that cannot be separated radiochemically [for instance (n,d) and (n,np)] can be studied separately if the charged particles are detected.

The present alpha-particle measurements are related also to helium accumulation measurements in which the quantity of helium produced by neutron bombardment is determined by mass spectro-metric methods.[3,4] Helium accumulation measurements yield energy and angle-integrated helium-production cross sections. In contrast to the radiochemical measurements, there is no requirement that the final nucleus reached by alpha decay be unstable, and natural isotopic mixtures or compounds may be studied. As in the case of radiochemical measurements, however, the direct determination of helium production does not give information on the energy or angular distribution of the alpha particles. Mass spectrometric methods have not yet been used to determine hydrogen production.

The nuclides studied in the present experiments are separated isotopes of Cr, Fe, Ni, and Cu, as well as natural Cr, Fe, and Ni. The choice of targets was influenced by their use in structural materials, especially in stainless steel. In addition, the target nuclides differ little in atomic mass, a fact that aids in the study of the reaction mechanism.

II. EXPERIMENTAL PROCEDURE

The charged-particle-emission cross sections were measured by detecting the protons, deuterons and alpha particles with a magnetic quadrupole spectrometer (Fig. 1).[5] This spectrometer consisted of a magnetic quadrupole triplet lens to transport the charged particles, and $\Delta E - E$ silicon surface barrier detectors to identify the particle type and to determine the particle energy.

The magnetic lenses focused the charged particles from their point of origin in the thin target foil onto the detectors 2.65 m away. This large distance, as well as shielding between the source and the detectors, reduced background counts and radiation damage in the detectors. In pre-

TABLE I. Target foils and composition.

Target foil	Thickness (mg/cm²)	Principal isotopic constituents $A(\%)$	Energy loss in half thickness of foil (MeV)	
			5-MeV proton	5-MeV alpha particle
^{50}Cr	3.5	50(95.9),52(3.8)	0.08	0.8
^{52}Cr	2.1	52(99.9)	0.05	0.5
Cr	2.3	50(4.3),52(83.8),53(9.5),54(2.4)	0.05	0.5
^{54}Fe	5.0	54(96.8),56(3.0)	0.12	1.3
^{56}Fe	5.0	56(99.9)	0.12	1.3
Fe	2.9	54(5.8),56(91.7),57(2.2)	0.07	0.8
^{58}Ni	4.8	58(99.9)	0.11	1.2
^{60}Ni	4.0	60(99.8)	0.10	1.0
Ni	5.7	58(67.8),60(26.2),61(1.2),62(3.7),64(1.1)	0.13	1.5
^{63}Cu	3.9	63(99.9)	0.08	0.9
^{65}Cu	4.0	65(99.7)	0.09	0.9

TABLE II. Geometry and mean neutron energy.

Angle between the incident neutron and the emitted charged particle (deg)	Angle between the incident deuteron and the emitted neutron (deg)	Source-to-target distance (cm)	Mean neutron energy and estimated half-width at half-maximum (MeV)
22	68	10.8	14.4 ± 0.2
30	60	8.0	14.5 ± 0.3
45	45	7.1	14.7 ± 0.4
76	14	5.4	$15.0 \, ^{+0.2}_{-0.4}$
90	0	5.0	$15.2 \, ^{+0.2}_{-0.4}$
104	14	5.4	$15.0 \, ^{+0.2}_{-0.4}$
135	45	7.1	14.7 ± 0.4

vious work[1,2,6] a magnetic quadrupole doublet lens was used. The triplet employed in the present experiment has better focusing properties.

The solid state counters were two silicon surface barrier detectors, 15 μm and 1500 μm thick, spaced 19 mm apart. These detectors had areas of 50 mm². Tantalum diaphragms decreased the effective areas to 38 mm² to reduce edge effects. The transmission detector could stop 0.9-MeV protons or 3.5-MeV alpha particles. The measured energy loss in the transmission detector served to identify the particles.

Neutrons from the $d + {}^3H$ reaction were generated by bombarding a rotating titanium tritide target[7] with 400-keV deuterons. The generator was usually operated at a source strength of 3×10^{12} n/s. Although neutrons emitted at 90° with respect to the incident deuterons have the energy of greatest interest to the fusion reactor application (14.1 MeV), the geometry of the rotating target precluded the use of these neutrons. Instead, the neutron production angle varied from 0° to 75°.

The neutrons produce the observed charged particles in thin, circular, self-supporting target foils. The foils used in the present measurements are listed in Table I. They were 2.5 cm in diameter. A diaphragm reduced the effective diameter to 2 cm to avoid contaminants from the foil holders.

One would ordinarily measure the angular distribution of the emitted charged particles by moving the detector around the foil. The size of the magnetic transport system and the neutron source configuration made such a procedure difficult. Different reaction angles were obtained instead by moving the transport system along its axis as shown in Fig. 1. This procedure has the disadvantage that the neutron energy varies with reaction angle. Table II gives the center of source to center of foil distances and the mean neutron energy for the reaction angles studied.

The central reaction angle was known to $\pm 1.5°$

at the most forward angle and to $\pm 3°$ at the 90° reaction angle. The angular range sampled at each position is a complicated function of the particle energy and the magnetic lens settings. The target foil subtended $\pm 3°$ to $\pm 5°$ about the central angle. The angular acceptance of the spectrometer increased the angular range sampled to an estimated $\pm 7°$.

The mean neutron energy varied as a function of angle from 14.4 to 15.1 MeV. This variation introduced some uncertainty in the interpretation of the data in cases where the cross section varies rapidly with neutron energy, such as in the reaction ${}^{58}Ni(n,p){}^{58}Co$. In general, the proton-emission cross section, which includes $(n,p) + (n,np) + \cdots$, would be expected to change less rapidly with energy than the individual (n,p) cross section for a particular nuclide.

The magnetic lens transport system permits charged particles within a band of momenta to reach the detector. Nine different settings of the currents through the magnet coils were required to cover the entire spectrum of emitted charged
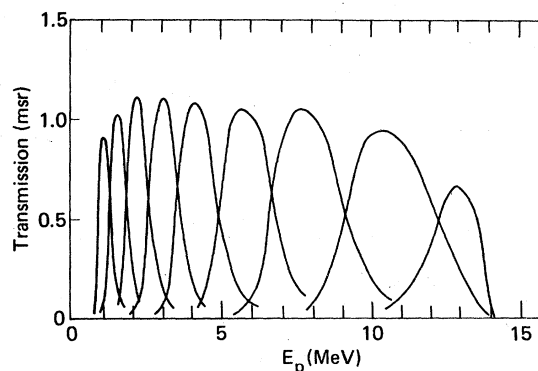
FIG. 2. Measured transmissions of protons for nine magnet current settings. The transmissions are expressed as effective solid angles for accepting protons emitted from the target foil.

particles. The transmission band of the system was measured for protons by observing the continuous spectrum of protons emitted from a thick polyethylene radiator. For each current setting the energy distribution of the protons was observed at the detector. This distribution was divided by the known energy distribution of the protons from the radiator. The measured transmission takes into account the efficiency of the detector system which is less than one for the most energetic protons, because these protons produce such a small signal in the transmission detector that they may be missed. For deuterons and alpha particles, however, the detector efficiency is nearly 100%. Figure 2 shows examples of such measurements. The transmissions are expressed as effective solid angles for the acceptance of protons from the radiator. The transmission bands for deuterons and alpha particles were determined with a thick CD_2 radiator. At a given magnet setting the system transports protons and alpha particles of the same energy and deuterons of half this energy. Thus, the transmission function for deuterons was shifted by a factor of 2 in energy for use in evaluating alpha-particle cross sections. This procedure for determining the transmission functions experimentally normalizes the cross sections to the n-p and n-d elastic-scattering cross sections and eliminates the need for an absolute flux determination.

The data shown in Fig. 3 were taken with the transmission band centered at 4.2 MeV, and were accumulated in 16 min. In addition, Fig. 3 shows the background measured without the foil. A typical charged-particle spectrum is shown in Fig. 4.
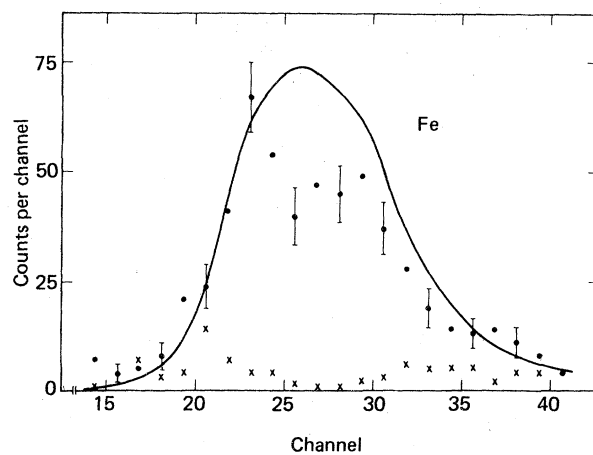
FIG. 3. Pulse height distributions (taken at 30°) with the quadrupole triplet set to focus 4.2-MeV protons. Dots represent data taken with the 3.0 mg/cm^2 natural iron foil, crosses data taken without the foil. The solid line is the transmission function. The error bars represent the statistical uncertainties only.
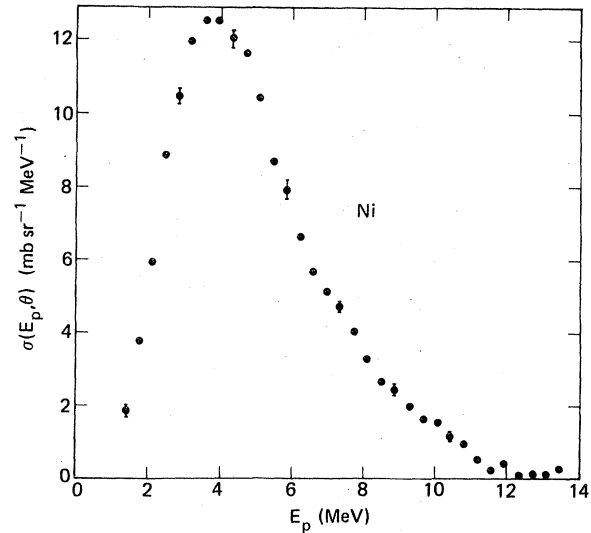
FIG. 4. Proton-emission cross sections at 90° for the 5.7 mg/cm^2 natural nickel foil. This distribution was obtained from data taken at nine different magnet settings. The error bars represent the statistical uncertainties only.

These data represent the results of nine separate gradient settings.

III. RESULTS

The differential energy spectra were summed in 500-keV bins and integrated over angle. Differential cross sections resulting from this integration are shown in Figs. 5–7. Further summation over outgoing energy yielded the total emission cross sections for protons, deuterons, and alpha particles; these values, as well as the average energies of the emitted charged particles, are listed in Table III.

Calculation of absolute cross sections requires knowledge of the neutron flux, target foil thickness, and the solid angle of the spectrometer. In our experimental technique the product of the spectrometer solid angle and the absolute neutron flux was determined by measuring a spectrum from a stopping sample of CH_2 or CD_2. Uncertainties in this product are due to errors in the stopping power of polyethylene (estimated to be less than 3%), errors in the cross sections for elastic scattering of neutrons from hydrogen and deuterium (10% for n-d including the angular uncertainty and less than 1% for n-p), and errors in the ratio of the solid angle of the target relative to the neutron source for the CH_2 or CD_2 compared to that for the metal foils. This latter uncertainty is estimated to be 8% and is due to the uncertainty in the distance between the neutron source and the radiator. Additional contri-
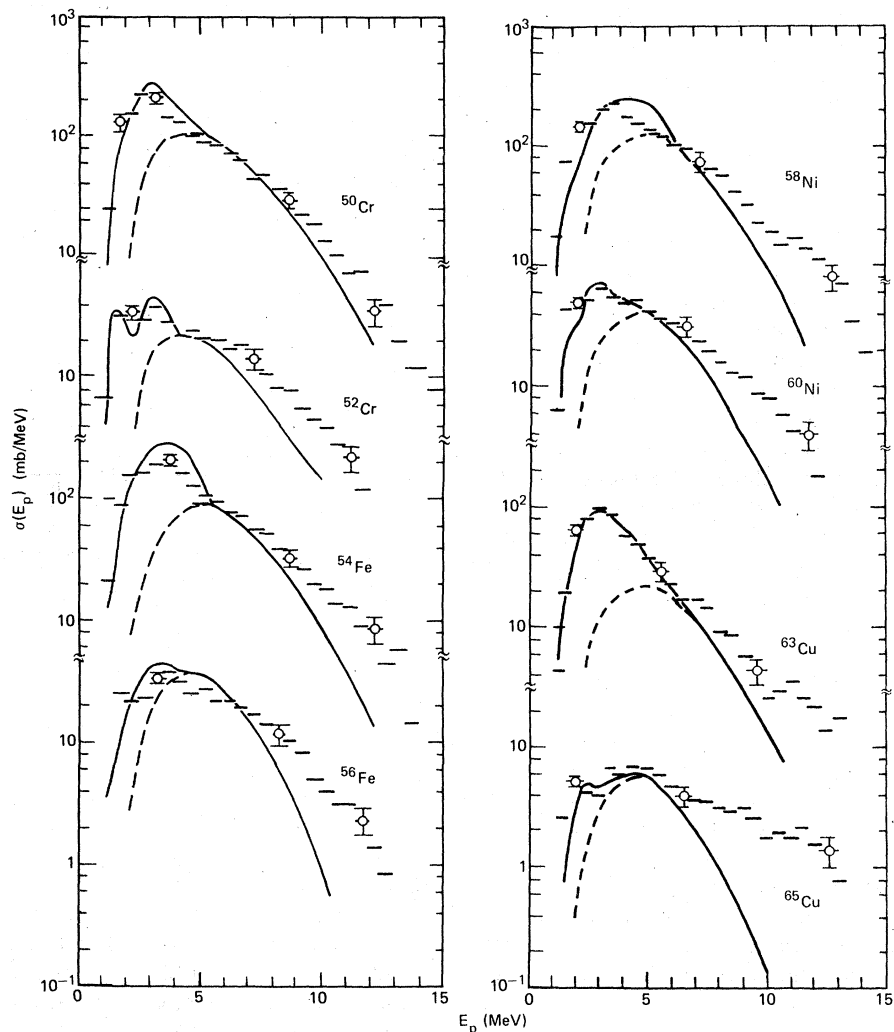
FIG. 5. Angle-integrated proton-emission cross sections for reactions induced by 14.8-MeV neutrons on targets of ^{50}Cr, ^{52}Cr, ^{54}Fe, ^{56}Fe, ^{58}Ni, ^{60}Ni, ^{63}Cu, and ^{65}Cu. The horizontal bars denote the experimental values averaged in 500-keV bins. Typical errors in the cross sections are shown. The multistage Hauser-Feshbach calculation is represented by a solid line. A dashed line indicates the calculated contribution from protons emitted by the first compound nucleus in the region where (n,np) and $(n,2p)$ are also energetically allowed.

butions to the cross section uncertainty come from target foil thickness errors (2.5%) and the combined effect of statistics and the uncertainty in obtaining a total cross section from a Legendre-polynomial fit to the cross section at a limited number of angles. The combined contribution of the latter two factors is typically 7% for proton and alpha-particle cross sections and 15% for deuteron cross sections. These errors were combined in quadrature. An additional 4% error was included for the alpha-particle cross sections because of the possibility that multiple scattering in the ΔE detector might not be exactly equal for alphas of energy E and deuterons of energy $E/2$, thus increasing the uncertainty in the use of deuteron

transmission functions for alpha particles. The combined errors were 11–15% for protons, 15–20% for alpha particles, and 20–30% for deuterons.

Energy spectra were corrected for energy loss in the target foil by assuming that all reactions took place in the central plane of the target foil. This assumption causes no difficulty for high charged-particle energies where the correction is small. At the lowest charged-particle energies, however, the spectrum is somewhat distorted. The energy-integrated cross section would not be affected by this uncertainty.

Cross sections presented in Figs. 5–7 are all in the laboratory system. Because the target nuclei have large masses, the angle-integrated
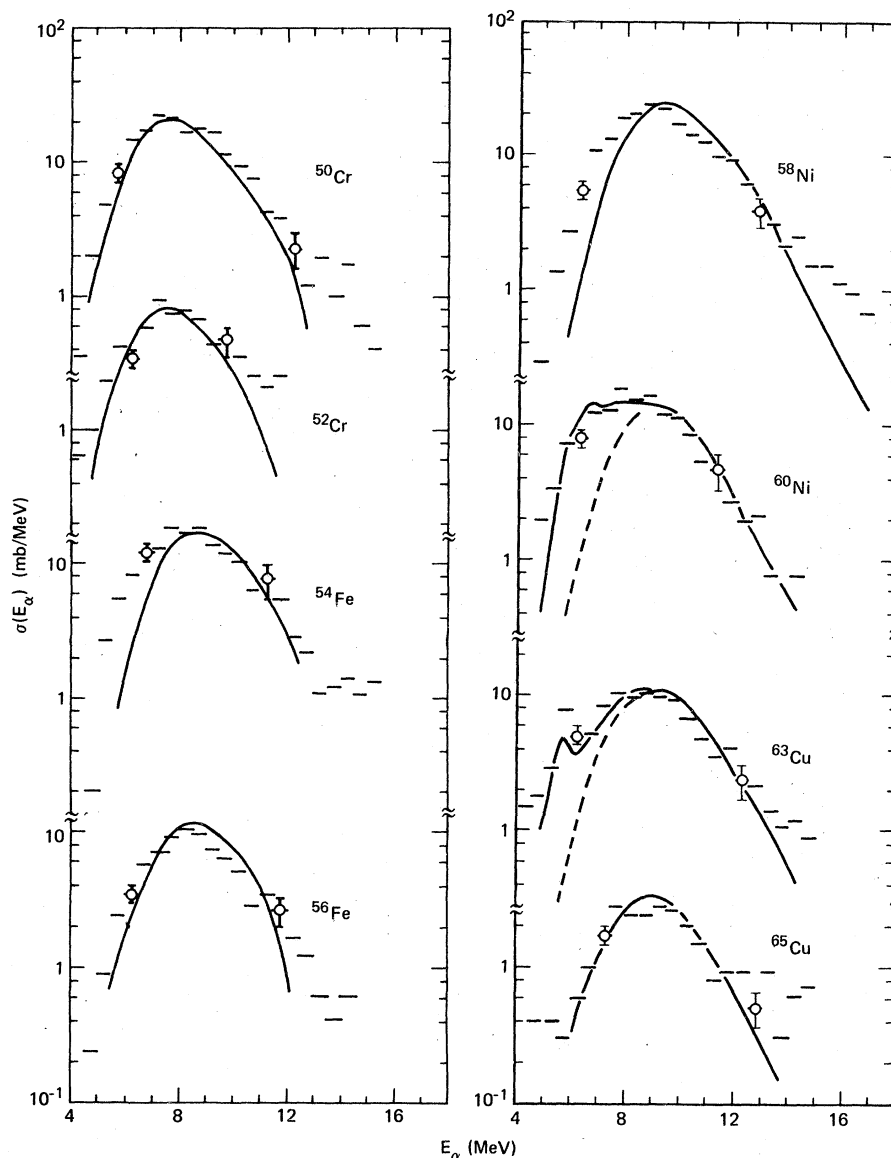
FIG. 6. Same as Fig. 5 for alpha-particle emission. The dashed line denotes the contribution from alpha particles emitted from the first compound nucleus.

differential energy spectrum in the center-of-mass system should be quite similar to the laboratory-system results presented here. Conversion of these results to the center of mass is complicated by the contributions from reactions that result in a three-particle final state.

Although cross sections were measured only at a few angles, they show systematic variations with angle as illustrated for ^{50}Cr in Fig. 8. This figure shows the variation of the ratios of the cross sections for proton, deuteron, and alpha-particle emission, to that at 30° for 1-MeV energy bands of the emitted particles. The distributions

for 3-MeV protons and 8-MeV alpha particles are isotropic within the uncertainty of the measurement, while the distributions for 10-MeV protons and 12-MeV alpha particles, as well as for deuterons, are strongly forward peaked. This suggests that the most energetic protons and alpha particles and the deuterons are produced in direct or pre-equilibrium processes.

Numerical values of the charged-particle-emission cross sections and spectra for the different emission angles are available from the National Nuclear Data Center, Brookhaven National Laboratory, Upton, N. Y. 11973.
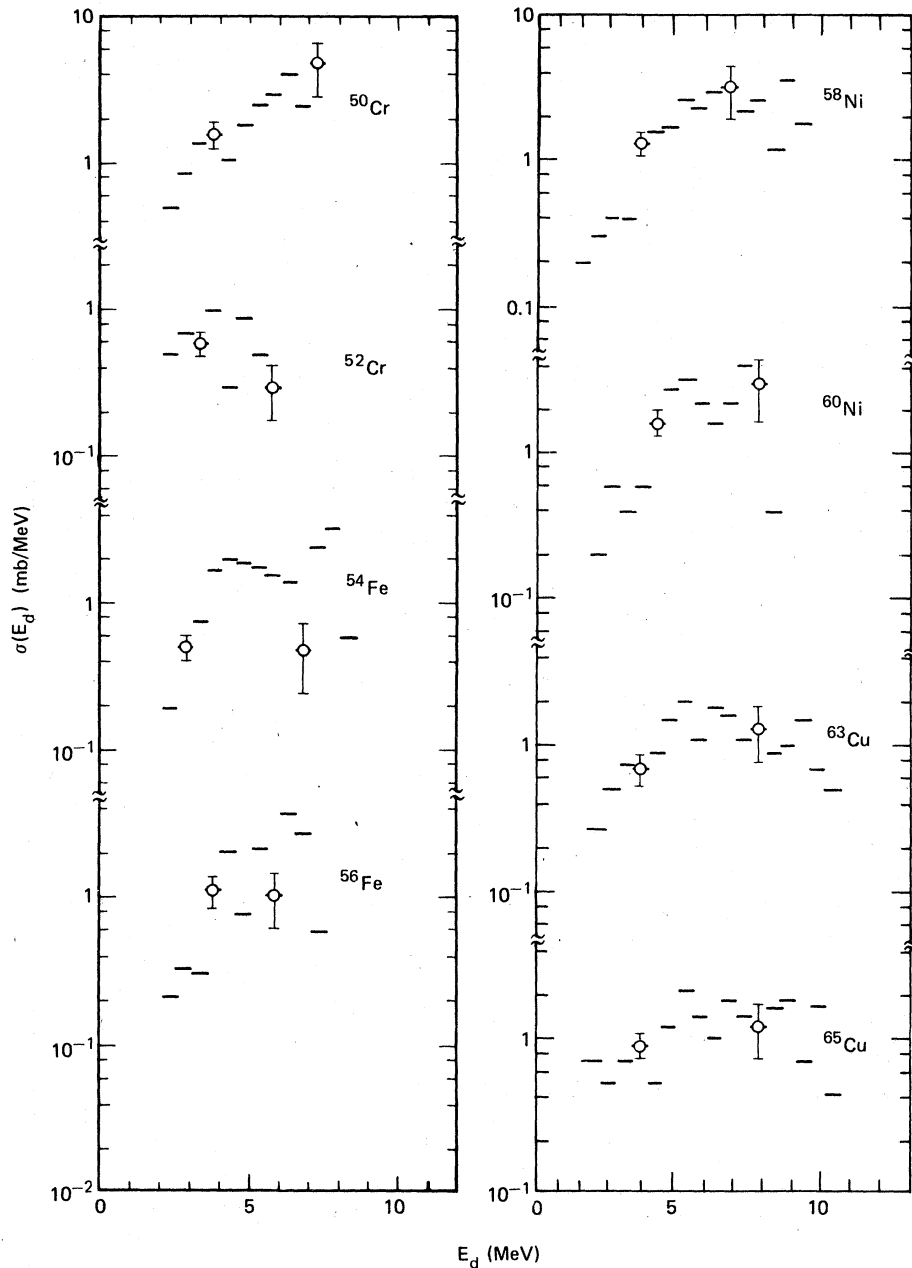
FIG. 7. Angle-integrated deuteron-emission cross sections for reactions induced by 14.8-MeV neutrons on targets of ^{50}Cr, ^{52}Cr, ^{54}Fe, ^{56}Fe, ^{58}Ni, ^{60}Ni, ^{63}Cu, and ^{65}Cu.

IV. COMPARISON WITH PREVIOUS MEASUREMENTS

Cross sections obtained in the present measurements may be compared with previous spectral measurements, direct helium-production determinations, and radiochemical data.

Table III lists the cross sections determined in the present experiment. Also shown for comparison are measurements by Farrar et al.[3] of the helium-production cross sections for 15-MeV

neutrons incident on natural iron, nickel, and copper. These measurements should be comparable to ours, since in both measurements the emission of alpha particles is observed regardless of the emission of other particles. A similar measurement for Cu by Holt et al.[4] is also given in Table III. The present data and those in Refs. 3 and 4 agree within errors, although the cross sections of Ref. 3 are slightly larger.

Measurements of proton- or deuteron-emission

TABLE III. Proton, deuteron, and alpha-particle-emission cross sections and average charged-particle energy.

Target	Particle emitted	Present data	Cross section (mb) Other measurements	Ref.	Spectrum-averaged charged-particle energy (MeV)
^{50}Cr	p	830 ± 100	430	8	4.5 ± 0.2
^{50}Cr	d	12 ± 4			5.6 ± 0.6
^{50}Cr	α	94 ± 15			8.4 ± 0.3
^{52}Cr	p	180 ± 25			4.7 ± 0.2
^{52}Cr	d	8 ± 3			4.9 ± 0.7
^{52}Cr	α	36 ± 6			8.4 ± 0.4
Cr	p	180 ± 25			4.7 ± 0.2
Cr	d	10 ± 3			5.7 ± 0.7
Cr	α	38 ± 6			8.6 ± 0.4
^{54}Fe	p	900 ± 110	600	8	4.8 ± 0.2
^{54}Fe	d	10 ± 4			5.6 ± 0.6
^{54}Fe	α	79 ± 13			8.7 ± 0.4
^{56}Fe	p	190 ± 22	121	8	5.1 ± 0.2
^{56}Fe	d	8 ± 3			5.5 ± 0.7
^{56}Fe	α	41 ± 7			8.8 ± 0.6
Fe	p	230 ± 30			5.0 ± 0.2
Fe	d	8 ± 3			5.4 ± 0.8
Fe	α	43 ± 7	48 ± 3	3	8.8 ± 0.4
^{58}Ni	p	1000 ± 120	773,830,422	8,9,10	5.1 ± 0.2
^{58}Ni	d	14 ± 6	25	9	6.5 ± 0.7
^{58}Ni	α	106 ± 17			9.5 ± 0.3
^{60}Ni	p	325 ± 40	185	8	5.0 ± 0.2
^{60}Ni	d	11 ± 4			6.0 ± 0.8
^{60}Ni	α	76 ± 12			9.0 ± 0.3
Ni	p	790 ± 100			4.9 ± 0.2
Ni	d	13 ± 5			6.3 ± 0.6
Ni	α	97 ± 16	98 ± 6	3	9.2 ± 0.4
^{63}Cu	p	320 ± 45	257	8	4.4 ± 0.2
^{63}Cu	d	9 ± 4			6.4 ± 0.7
^{63}Cu	α	56 ± 10			8.9 ± 0.3
^{65}Cu	p	44 ± 5			6.2 ± 0.3
^{65}Cu	d	10 ± 4			6.6 ± 0.8
^{65}Cu	α	13 ± 3			9.5 ± 0.7
Cu	p	237 ± 28 [a]			5.0 ± 0.3 [a]
Cu	d	10 ± 4 [a]			6.5 ± 0.8 [a]
Cu	α	42 ± 7 [a]	$51 \pm 3, 54 \pm 5$	3,4	9.1 ± 0.4 [a]

[a] Inferred from isotopic data.

cross sections through differential energy spectra have been reported for some of these nuclei by Allan,[8] Glover and Purser,[9] and Alvar.[10] The cross section measured in Ref. 9 for the ^{58}Ni(n,d) reaction is larger than the present value, while the proton-emission cross section for ^{58}Ni is slightly smaller. All of the values of Ref. 8 are smaller than the present results. This disagreement is probably due to Allan's assumption that the angular distributions were isotropic (cf. Fig. 8 for a typical angular distribution) and to the extrapolation for protons emitted with energies below 2 MeV. The proton-emission data for ^{58}Ni of Ref. 10 are below the present value, both because of the 2-MeV cutoff and the omission of angles beyond 120°.

Comparison of our results with radiochemical determinations is difficult because, in the radiochemical measurements, specific residual nuclides are observed rather than the light charged particles. Table IV lists some activation measurements on targets for which some comparisons can be made as well as the recommended values listed in Refs. 11, 12, and 13. In no case are enough activation cross sections available to compare all of the charged-particle cross sections for a specific target. If the cross sections for $(n, 2\alpha)$ and $(n, \alpha p)$ are assumed to be small, the total alpha-particle-emission cross section should be approximately equal to the sum of the (n, α) and the $(n, n\alpha)$ cross sections; the values of Ref. 18 for ^{65}Cu agree with our result. For some other targets, data on the
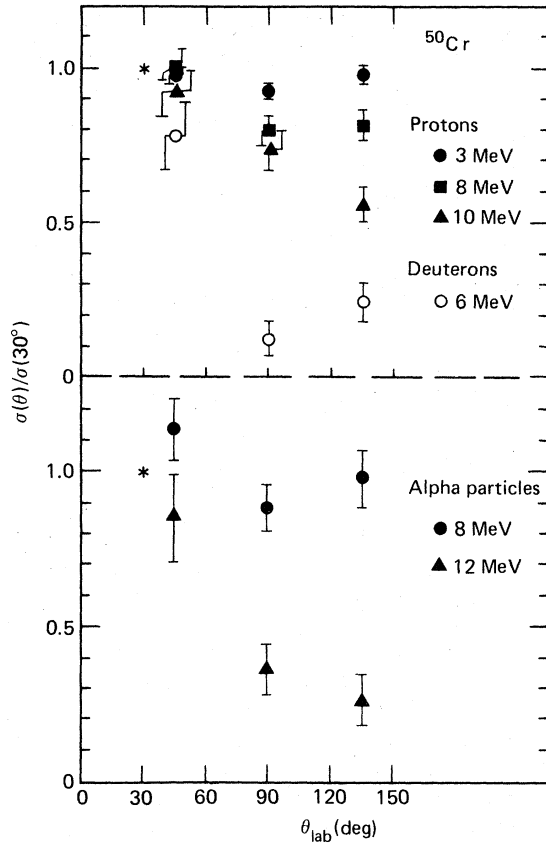
FIG. 8. Variation with angle of the cross sections for the emission of protons, deuterons, and alpha particles from the bombardment of ^{50}Cr with 14.8-MeV neutrons. The cross sections are normalized to unity at 30°. The charged particles are measured in 1-MeV bins centered around the indicated energy.

(n, α) cross sections are available and give a lower limit for the total alpha-particle-emission cross section. For ^{54}Fe and ^{58}Ni, our values are slightly lower than this limit, but agree with it within the errors. The ^{63}Cu(n, α) cross section listed in Table IV is less than our measured alpha-particle-emission cross section, hence the ^{63}Cu$(n, n\alpha)$ cross section is probably appreciable. The shape of the alpha-particle spectrum near 5 MeV (Fig. 6) also suggests a $(n, n\alpha)$ contribution.

Similarly, radiochemical determinations of (n, p) cross sections can give lower limits for the total proton-emission cross section. For ^{52}Cr, ^{54}Fe, ^{56}Fe, ^{58}Ni, ^{60}Ni, and ^{65}Cu the radiochemical values are significantly less than the corresponding proton-emission cross section. This does not represent an inconsistency but rather serves as another indication of the importance of the (n, np) reaction. Since the $(n, np +d)$ cross section is available for ^{58}Ni, a lower limit of from 828 to 1080 mb [depending on which values are used for

TABLE IV. Radiochemical determinations of cross sections.

Reaction	Cross section (mb)	Ref.
^{52}Cr$(n, p)^{52}$V	96 ± 10	12
	80 ± 6	13
^{54}Fe$(n, p)^{54}$Mn	290	11
	315 ± 25	13
^{54}Fe$(n, \alpha)^{51}$Cr	96 ± 10	13
^{56}Fe$(n, p)^{56}$Mn	99.4	11
	103 ± 6	12
	98 ± 7	13
	109 ± 9	14
^{58}Ni$(n, p)^{58}$Co	316	11
	330 ± 30	12
	248	15
^{58}Ni$(n, np + d)^{57}$Co	593	15
	750 ± 60	13
	580	16
^{58}Ni$(n, \alpha)^{55}$Fe	125 ± 15	13
^{60}Ni$(n, \alpha)^{57}$Fe	110	11
	109 ± 8	12
	100 ± 9	13
^{63}Cu$(n, p)^{63}$Ni	118 ± 20	12
^{63}Cu$(n, \alpha)^{60}$Co	31 ± 2.2	17
	33	9
^{65}Cu$(n, p)^{65}$Ni	29.3 ± 3.2	18
	23 ± 3	12
^{65}Cu$(n, \alpha)^{62}$Co	16 ± 10	18
	11 ± 5	12
^{65}Cu$(n, n\alpha)^{61}$Co	2.9 ± 8	18

(n, p) and (n, np)] may be deduced for the sum of proton and deuteron emission from ^{58}Ni. Calculations based on Hauser-Feshbach theory with the parameters given in the next section predict an $(n, 2p)$ cross section of 36 mb, so that the total proton-emission cross section ought to exceed the lower limit by about 70 mb. Thus, radiochemical values for the ^{58}Ni target agree with the present measurements within the quoted errors.

In summary, in the cases where comparisons can be made, the present data are consistent with data from other types of measurements, such as radiochemical or helium accumulation experiments.

V. COMPARISON WITH CALCULATIONS

Previous studies[1,2] of neutron-induced charged-particle-producing reactions at 15 MeV in this mass region have shown that proton and alpha-particle emission proceeds largely through compound-nuclear reactions, while (n, d) reactions are primarily direct. The present measurements are consistent with this pattern in that the proton and alpha-particle emission is nearly isotropic and is quite sensitive to neutron binding energies. Deuteron emission, in contrast, is strongly forward peaked as shown in Fig. 8, and shows much
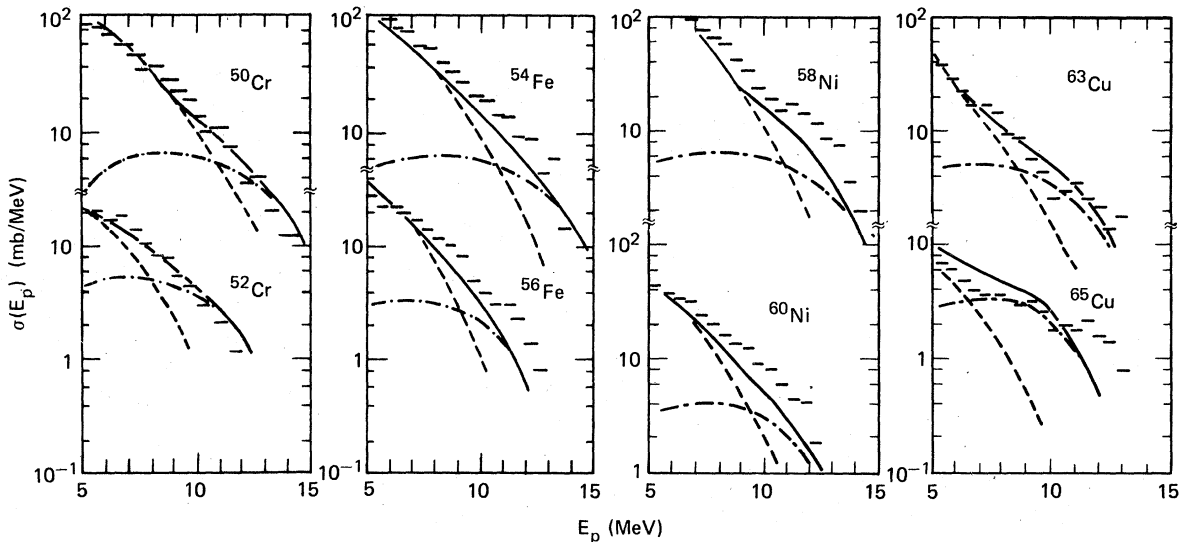
FIG. 9. High-energy portions of the proton-emission cross sections shown in Fig. 5 are compared with hybrid-model calculations (dot-dashed line), multistep Hauser-Feshbach calculations (dashed line), and the sum of these two contributions (solid line).

smaller variation from isotope to isotope.

To investigate the question of reaction mechanism in more detail, Hauser-Feshbach calculations were performed for the separated isotope targets. Details of the computer code used and the procedure for determining level-density parameters have already been published.[19] Transmission coefficients for neutrons, protons, and alpha particles were obtained from optical model parameters proposed by Wilmore and Hodgson,[20] Becchetti and Greenlees,[21] and Huizenga and Igo,[22] respectively. γ-ray transmission coefficients were taken from the work of Woosley *et al.*[23] As has been pointed out previously,[2] it is important to use known level schemes for the lowest few MeV of excitation of the residual nuclide. When they were known, the lowest fifteen to twenty levels were used for each residual nuclide and a continuum was employed at higher energies.

The spectra calculated under these assumptions are shown in Figs. 5 and 6. Agreement with the data is generally good. The statistical calculations reproduce all but the highest-energy portions of the proton and alpha-particle spectra. Multistage statistical calculations have been found[2] to describe the sub-Coulomb-barrier peak observed in proton-emission spectra if the γ-ray channel is included at the second stage of the reaction. This conclusion is supported by the present comparisons. For the targets ^{50}Cr, ^{54}Fe, and ^{58}Ni, the low-energy peaks contain about 40% of the total proton production cross section. The substantial cross section in this energy region underscores the need for measuring charged particles of low energy

to determine the total charged-particle-emission cross sections.

In addition, the even-A targets show larger contributions from (n,np) reactions than the odd-A targets, even when the binding energy differences between protons and neutrons are similar; this conclusion is consistent with the results reported in Ref. 2 and is due primarily to the paucity of low-lying states in the even-even final nuclides reached by the (n,np) reaction on odd-Z–odd-A targets.

The number of alpha particles tend to be somewhat larger at low energies than the predictions. Some of this difference may be due to the treatment of the experimental data: The low-energy portion of the experimental alpha-particle spectrum is smeared out because the measurements are corrected for energy loss in the target in a simplified fashion and because the data are in the laboratory system while the calculations are in the center-of-mass system. The fact that the summed measured cross sections in this region are larger than the calculated cross sections, however, may imply that the use of a global prescription for the γ-ray transmission coefficients is not correct for some nuclides in calculating $(n,n\alpha)$ cross sections. The proton data have a similar tendency to be larger than the calculations for small emission energies, but in this case the differences are smaller and may again be due to the energy loss and center-of-mass-to-laboratory corrections. Further investigations will be necessary to determine whether these differences are significant and whether changes in the multistep Hauser-Feshbach calcula-

tions are required.

The proton-emission spectra were also compared with the predictions of the hybrid model[24] for pre-equilibrium reactions. Addition of this component significantly improves the agreement of the calculated with the experimental spectrum in the region of highest proton energy (Fig. 9). In each case the predicted pre-equilibrium decay is about 12% of the total reaction cross section. Roughly 40% of this pre-equilibrium decay takes place by proton emission, with the remainder by neutron emission.

The cross section for proton emission from pre-equilibrium states varies less rapidly with the relative neutron and proton binding energies than does the corresponding cross section for equilibrium processes. This difference is due to the fact that the total width of an equilibrium state is due to particle and γ decay, while the largest part of

the width of a pre-equilibrium state is due to decay to more complicated states. Thus, changes in the number of final states in the residual nucleus reached by neutron emission affect the pre-equilibrium cross section less than the equilibrium cross section. Because the branching ratio for proton decay from equilibrium states in neutron-rich targets is small, the pre-equilibrium component in the proton-emission cross section is more important than the small pre-equilibrium decay fraction would suggest. For all targets included in the present study, however, equilibrium reactions still produce more than half of the protons observed.

*Currently on leave at the Department of Physics, Ohio University, Athens, Ohio 45701.

†Present address: IRT Corporation, San Diego, Calif. 92138.

‡Currently on leave at the University of Colorado, Boulder, Colo. 80309.

[1]S. M. Grimes, R. C. Haight, and J. D. Anderson, Nucl. Sci. Eng. 62, 187 (1977).

[2]S. M. Grimes, R. C. Haight, and J. D. Anderson, Phys. Rev. C 17, 508 (1978).

[3]H. Farrar IV, and D. W. Kneff, Trans. Am. Nucl. Soc. 28, 197 (1978).

[4]J. B. Holt, D. W. Hosmer, and R. A. Van Konynenburg, in International Conference on Radiation Effects and Tritium Technology for Fusion Reactors, Gatlinburg, Tenn., Conf., edited by J. S. Watson and F. W. Wiffen (USERDA, Conf-750989, 1975), Vol. II, p. 280.

[5]K. R. Alvar, H. H. Barschall, R. R. Borchers, S. M. Grimes, and R. C. Haight, Nucl. Instrum. Methods 148, 303 (1978).

[6]R. C. Haight, S. M. Grimes, B. J. Tuckey, and J. D. Anderson, Lawrence Livermore Laboratory Report No. UCRL-77151, 1975 (unpublished).

[7]R. Booth and H. H. Barschall, Nucl. Instrum. Methods 99, 1 (1972).

[8]D. L. Allan, Nucl. Phys. 24, 274 (1961).

[9]R. N. Glover and K. H. Purser, Nucl. Phys. 24, 431 (1961).

[10]K. R. Alvar, Nucl. Phys. A195, 289 (1972).

[11]B. A. Magurno et al., ENDF/B-IV Dosimetry File, Brookhaven National Laboratory Report No. BNL-NCS-50446, 1975 (unpublished).

[12]M. Bormann, H. Neuert, and W. Scobel, Tables and Graphs of Cross Sections for (n,p), (n,α), and $(n,2n)$ Reactions in the Neutron Energy Region 1–37 MeV, in Handbook on Nuclear Activation Cross Sections (IAEA, Vienna, 1974), pp. 87–272.

[13]S. M. Qaim and N. I. Molla, Proceedings of the Ninth Symposium on Fusion Technology, Garmisch (Pergammon, Oxford, 1976), pp. 589–595.

[14]R. C. Barrall, M. Silbergeld, and D. G. Gardner, Nucl. Phys. A138, 387 (1969).

[15]P. Guenther, A. Smith, D. Smith, J. Whalen, and R. Howerton, Argonne National Laboratory Report No. ANL/NDM-11, 1975 (unpublished).

[16]R. N. Glover and E. Weigold, Nucl. Phys. 29, 309 (1962).

[17]H. Liskien and A. Paulsen, Nucl. Phys. 63, 393 (1965).

[18]E. T. Bramlitt and R. W. Fink, Phys. Rev. 131, 2649 (1963).

[19]S. M. Grimes, J. D. Anderson, J. W. McClure, B. A. Pohl, and C. Wong, Phys. Rev. C 10, 2373 (1974).

[20]D. Wilmore and P. E. Hodgson, Nucl. Phys. 55, 673 (1964).

[21]F. D. Becchetti and G. W. Greenlees, Phys. Rev. 182, 1190 (1969).

[22]J. R. Huizenga and G. Igo, Nucl. Phys. 29, 462 (1962).

[23]S. E. Woosley, W. A. Fowler, J. A. Holmes, and B. A. Zimmerman, California Institute of Technology Report No. OAP-422, 1976 (unpublished).

[24]M. Blann, Phys. Rev. Lett. 27, 337 (1971); Nucl. Phys. A213, 570 (1973).